Arabian Journal of Chemistry (2021) **14**, 103351

King Saud University

Arabian Journal of Chemistry

www.ksu.edu.sa
www.sciencedirect.com

ORIGINAL ARTICLE

An amphiphilic fluorogen with aggregation-induced emission characteristic for highly sensitive and selective detection of Cu^{2+} in aqueous solution and biological system

Deqiang Wang [a], Xin Zhou [a], Chong Ma [a], Meiying Liu [a,c], Hongye Huang [a,b], Xiaoyong Zhang [a,*], Yen Wei [b,*]

[a] *Department of Chemistry, Nanchang University, Nanchang 330031, PR China*
[b] *Department of Chemistry and the Tsinghua Center for Frontier Polymer Research, Tsinghua University, Beijing 100084, PR China*
[c] *Jiangxi University of Traditional Chinese Medicine, Nanchang 330004, PR China*

Received 21 April 2021; accepted 21 July 2021
Available online 29 July 2021

KEYWORDS

Aggregation-induced emission;
Fluorescent sensor;
Self-assembly;
Heavy metal ions;
Water soluble fluorescent probes

Abstract Fluorescent sensor has demonstrated to be a facile and effective method to detect heavy metal ions owing to its unique characteristics such as simplicity, ease of operation and cost-effectiveness. In this work, a novel fluorescent probe with aggregation-induced emission (AIE) feature that contains an amide ligand base on the tetraphenylethylene (TPE) dye was designed and successfully synthesized. The utilization of the AIE-active fluorescent probe (named as FDPA) for detection of Cu^{2+} in aqueous solution has also been examined. We demonstrated that the resultant AIE-active molecule displays amphiphilic property and can self-assemble in aqueous solution with remarkable enhancement of fluorescent intensity owing to its AIE feature. The detection limit of probe for Cu^{2+} determination is 6.11×10^{-9} M and shows excellent selectivity in the presence of competitive ions. This work provides a useful route to overcome the fluorescence quenching of conventional fluorescent probes in aqueous solution and an elegant way to prepare fluorescent probes with better fluorescence properties.

1. Introduction

Copper is an essential micronutrient in human body. It plays an important role as structural component of many proteins in many biological processes owing to its redox-nature (Prohaska and Gybina, 2004; Que et al., 2008; O'Halloran, 2008). But accumulating excessive Cu^{2+} in living organisms can cause a series of diseases, just like Menkes, Alzheimer's, Wilson's diseases and prion diseases and so on (Barnham et al., 2004; Lutsenko et al., 2008; Aksuner et al., 2009). Moreover,

* Corresponding authors.
E-mail addresses: zhangxiaoyong@ncu.edu.cn (X. Zhang), weiyen@tsinghua.edu.cn (Y. Wei).

Peer review under responsibility of King Saud University.

Production and hosting by Elsevier

https://doi.org/10.1016/j.arabjc.2021.103351
1878-5352

since copper has become a kind of principal raw materials which used in industry and agriculture, it has turned into one of the most important environmental pollutants (Thavornpradit et al., 2016). As a consequence, how to selective detection and quantitative analysis of Cu^{2+} in complex aqueous environment condition is a crucial and important research subject. Many methods, such as inductively coupled plasma atomic emission spectrometry (ICP-AES) (Moreda, 2005), atomic absorption spectroscopy (Pourreza and Hoveizavi, 2005) and inductively coupled plasma mass spectrometry (ICP-MS) (Becker et al., 2007) and UV–vis spectrometer (Huang et al., 2018; Huang et al., 2018; Dou et al., 2019; Zhang et al., 2015) have been previously reported for detection of Cu^{2+}. However, these methods of copper ion detection are normally time-consuming, laborious and complicated, making them a definite limit applied to the detection fields. Fluorescent sensor technology is attracting more and more interest because of its advantages, such as cost-effective, nondestructive, simple operation, highly sensitivity and selectivity, etc. (Liu et al., 2012; Mahato et al., 2012). A series of Cu^{2+} selective fluorescent sensors have been reported previously (Kaur et al., 2016; Xue et al., 2016; Wang et al., 2017). Nevertheless, most of them often suffer from numerous problems such as low selectivity and sensitivity, water insolubility, interference from other metal ions (Situ et al., 2017; Park et al., 2014). More importantly, these conventional organic luminophores show high fluorescence in very dilute solution, but suffered a fatal deficiency of fluorescence quenching in high concentrations or aggregated state (Hong et al., 2011; Wang et al., 2016). It is also a renowned problem of many conventional organic molecules that was called the aggregation caused quenching effect (ACQ). Therefore, the development more efficient fluorescent probes with better fluorescence properties for detecting Cu^{2+} in aqueous solution is still highly desirable.

The aggregation-induced emission (AIE) is an abnormal fluorescence phenomenon that was obvious opposite with the ACQ of conventional fluorescent organic molecules. This interest fluorescence phenomenon was first discovered and purposed by Prof. Tang in 2001 (Xu et al., 2010) and it has been promptly applied to various fields because of its inimitable fluorescent properties, especially in the aspect of chemo-sensors (Sen Gupta et al., 2017; Li et al., 2016). In other word, the fluorescence organic molecules with AIE feature will emit more efficient in solid or aggregated state while no fluorescence or weak emission in well dispersed state (Shultz and Fox, 1989; Sun and Fox, 1993). It is therefore the fluorescent chemo-sensors based on AIE luminogens (AIEgens) are expected to display stronger fluorescence intensity in aqueous solution for the hydrophobicity and aggregation of AIEgens and therefore provide better sensor performance as compared with the fluorescent probes based on conventional fluorescent organic molecules (Kaur et al., 2016; Tong et al., 2006; Yu et al., 2017; Maurya and Singh, 2017; Shan et al., 2018; Liu and Qian, 2017; Yan et al., 2020; Kong et al., 2017; Wang et al., 2019). Although some reports have focused on the AIEgens based chemo-sensors, these fluorescence chemo-sensors are still at the early stage and the AIEgens used for chemo-sensors are normally poor dispersibility in aqueous solution (Zhang et al., 2013). While there are still some troubles when these chemo-sensors were utilized for sensors in pure aqueous solution and living organisms (Jiang et al., 2017; Jiang et al., 2017; Cao et al., 2017; Cao et al., 2017). Therefore, the synthesis of novel AIEgens with better aqueous dispersion should of great importance and interest. To the best of our knowledge, the chemo-sensor of heavy metal ions in aqueous solution using AIE-active probes has some reported thus far. In recently, some articles have reported that fluorescence probes with AIE characteristics can detect different heavy metal ions such as Cu^{2+}, Fe^{3+}, Hg^{2+} and Pb^{2+} (Yuan et al., 2019; Padhan et al., 2019; Shyamal et al., 2016; Khandare et al., 2014). For example, Liu et al have synthesized a new polymer probe TPE-CS through linked TPE with chitosan, which would detect Cu^{2+} (Liu et al., 2017). Qin et al have synthesized polyanetholesulfonic acid sodium salt with AIE activity (Qin et al., 2018). This probe could be used to detect Fe^{3+}. Jiang et al have synthesized a new AIEgen-based probe, m-TPE-RNS, which was used to detect Hg^{2+}. When the probe m-TPE-RNS was encountered Hg^{2+}, the probe was changed from m-TPE-RNS to m-TPE -RNO (Jiang et al., 2016).

In this contribution, the amphiphilic AIEgen (named as FDPA) was synthesized for the first time that contains the hydrophobic fluorescence segment (TPE) and hydrophilic heavy metal ions binding site (2-methylaminopyridine) and was utilized to selective sensor of Cu^{2+} in aqueous solution and living cells (Scheme 1). This probe displays excellent sensitivity to Cu^{2+} due to its unique optical mechanism restriction of intramolecular rotations (RIR). Because FDPA contains hydrophobic and hydrophilic components simultaneously, it can self-assembly to nanostructure and show the strong fluorescence of the probe in the solution of pure aqueous with high water dispersibility. The results in this paper demonstrated that FDPA could be used for detection of Cu^{2+} in nearly pure aqueous solution with high sensitivity and selectivity.

2. Experimental sections

2.1. Materials and instruments

4-Bromobenzophenone, 4-Aminobenzophenone, anhydrous THF, titanium tetrachloride, 2,2-Dichloroacetyl chloride, 4-Formylphenylboronic acid, 2-(Aminomethyl) pyridine and triethylamine, nitrate metal salts and Zinc chloride, ferric chloride, aluminum (III) chloride, copper (II) acetate and magnesium acetate were all purchased from Aladdin Company (Shanghai, China). Dichloromethane, sodium bicarbonate and acetonitrile were purchased from Tianjin Company, China. All reagents were analytical grade and were used without any further purification. (Prohaska and Gybina, 2004)H nuclear magnetic resonance (NMR) spectra were obtained on D_2O and $CDCl_3$ solution with Bruker Avance-400 spectrometer. All chemical shifts were reported in ppm and coupling constants (J) in Hz. The fluorescence data were obtained from the Fluorescence Spectrometer F-4600 which purchased from Hamamatsu (Japan). Dynamic laser scattering (DLS) experiments were performed on a Zeta Plus apparatus (Zeta Plus, Brookhaven Instruments, Holtsville, NY). UV–Visible spectra were acquired on a Persee TU-1810 spectrophotometer. The absolutely fluorescence quantum yield was determined by FLS1000 photoluminescence spectrometer (Edinburgh Instruments). The measurement method of LOD is shown in supporting information.

2.2. Synthesis of the probe

The synthesis of the AIE-active probe FDPA and its intermediates (BDPA, CDPA and CFDPA) was shown in Scheme 2 in detail. The procedures contained the synthesis of these molecules were described below.

2.2.1. Synthesis of BDPA

BDPA is synthesized by McMurry coupling reaction (Sen Gupta et al., 2017) and is a common modified coupling reaction, which is commonly used for aldehyde-ketone coupling. 4-bromo-diphenylketone and 4-benzoyl aniline have ketone groups and suitable functional groups, and are suitable as reaction materials. In a three-necked flask under nitrogen atmosphere, take zinc powder (as the reducing agent, 1.461 g, 22.33 mmol) and anhydrous THF (as solvent, 40 mL) were mixed in the flask with ice bath. After finishing

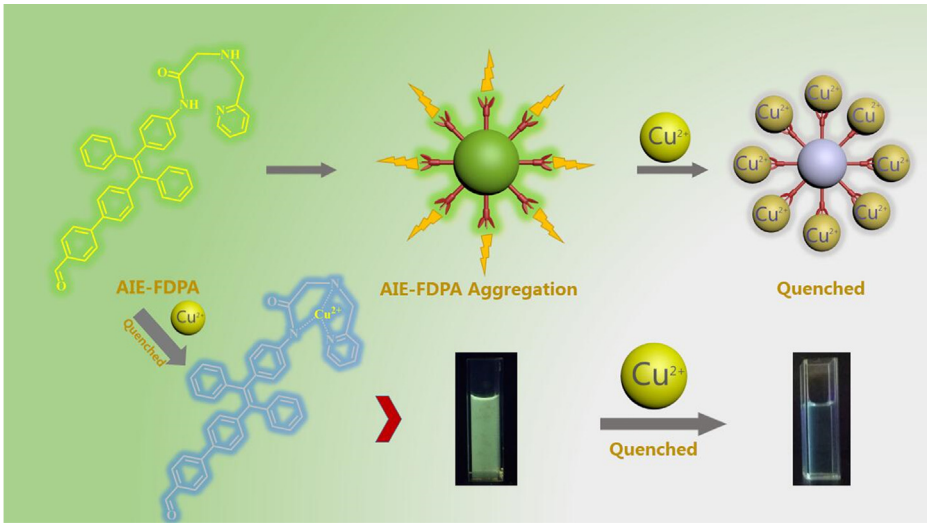

Scheme 1 The chemical structure of FPDA and its mechanism for Cu^{2+} sensor. Owing to the probe (FDPA) contains both the hydrophobic and hydrophilic segments, it can form AIE-FDPA aggregates after self-assembly. These fluorescent nano-aggregates could therefore display high fluorescence and well dispersibility in aqueous solution. On the other hand, the probe could coordinate with the metal ions and result in fluorescence quenching.

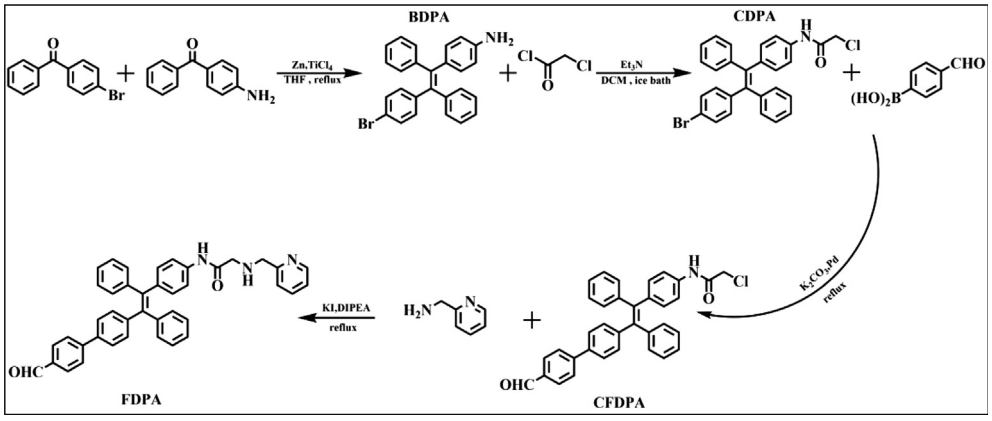

Scheme 2 The synthesis routes of BDPA, CDPA, CFDPA and FDPA.

that, the $TiCl_4$ (2.500 g, 13.18 mmol) was added slowly by a syringe. 4-bromo-benzophenon (0.783 g, 2.99 mmol) and 4-benzoylaniline (0.500 g, 2.53 mmol) were dissolved in THF (as solvent, 20 mL), and this solution of these reactants were added into the reaction solution at a slow rate. When the solution of these reactants is dripped, the reaction was needed to keep reacting about half an hour. After addition, the reaction flask was taken out from ice bath and then refluxed overnight. After the reaction has reached the scheduled time, the solution of K_2CO_3 aqueous solution was used to quench the reaction, then the organic layer of quench mixture solution was extracted with CH_2Cl_2. When finished above step, silica-gel chromatography was the way to purifying the crude product, petroleum ether and ethyl acetate were the eluent of the silica-gel chromatography, and the volume ratio of the eluent is 10:1. After completing above steps, the yield of the product reached 33%, and the color of product is light-yellow. ^1H NMR (300 MHz, $CDCl_3$), δ (TMS, ppm): 5.80 (s, 2H), 6.44 (m, 2H), 6.77 (m, 4H), 6.85 (d, 2H), 6.93 (d, 2H), 7.18 (d, 4H), 7.32 (d, 2H), 7.45 (d, 2H). (Dou et al., 2019)C NMR (100 MHz, $CDCl_3$ d6, TMS), δ(ppm): δ144.89, 143.95, 143.8, 143.73, 143.65, 143.3, 141.6, 133.02, 132.43, 131.35, 130.82, 130.7, 127.77, 127.72, 127.66, 127.53, 126.51, 126.40, 126.27, 119.9, 114.47, 114.37. ESI-MS (ESI, *m*/*z*): $[M^+]$ calcd of $C_{26}H_{20}BrN$, 425.08; found, 426.0834 $[M+H^+]^+$.

2.2.2. Synthesis of CDPA

This is a typical substitution reaction. Chloroacetyl chloride was reacted with the amine group of BDPA. Chloroacetyl chloride and BDPA lose chloride ion and hydrogen ion, respectively. CDPA was obtained via the following steps. The chloroacetyl chloride (0.160 g, 1.41 mmol) was dissolved in the solution of CH_2Cl_2 (as solvent, 20 mL), then BDPA (0.500 g, 1.17 mmol) and triethylamine (0.180 g, 1.77 mmol) was dissolved in the solution of CH_2Cl_2 (as solvent, 30 mL). Then, the solution of chloroacetyl chloride was slowly dropped into the solution containing BDPA and trimethylamine, and the solution of this reaction was stirred in ice bath for 1 h.

After that, the reaction flask was taken out from ice bath and then was warmed to room temperature for 2 h. In the next step, the solvent was removed under reduced pressure. When this step was finished, the light-yellow solid product was obtained. The silica-gel chromatography was used to purify the crude product. Petroleum ether and ethyl acetate with volume ratio of 5:1were used as the eluent of silica-gel chromatography. (Prohaska and Gybina, 2004)H NMR (400 MHz, $CDCl_3$), δ (TMS, ppm): 4.15 (d, J = 4 Hz, 2H), 6.87 (t, 4H), 7.0 (t, 4H), 7.10 (m, 4H), 7.21 (m, 2H), 7.33 (m, 2H), 7.45 (m, 2H), 8.14 (d, J = 7.08 Hz, 1H). (Dou et al., 2019)C NMR (100 MHz, $CDCl_3$ d6, TMS), δ(ppm): δ163.63, 143.1, 142.6, 140.9, 140.65, 140.35, 140.22, 139.79, 135.21, 135.07, 132.98, 132.01, 131.25, 130.95, 130.82, 127.9, 127.73, 127.82, 127.75, 126.7, 126.67, 42.9.

2.2.3. Synthesis of CFDPA

This reaction was a typical Suzuki coupling reaction (Li et al., 2014). Based on the previous related synthesis experiments, we found that the Suzuki reactivity of the chlorine group and the bromine group are quite different. In this reaction, the reaction activity of methyl chloride is low, while the reaction activity of bromine group is high. Phenylboronic acid and halogen group were reacted under Pd catalyst. The boric acid group and the halogen group were simultaneously removed, and the benzoyl group was connected to TPE. The emission color of the dye has changed from blue to yellow. In order to introduction of recognition group on the synthetic probe, 4-formylphenylboronic acid (0.18 g, 1.2 mmol) and CDPA (0.5 g, 1 mmol) were dissolved in the solution of THF (as solvent, 40 mL), and potassium carbonate aqueous solution (solution concentration is 2 mol/L) was added into the flask with CDPA solution. Under N_2 atmosphere, the reaction was maintained for half an hour at room temperature. After that, tetrakis (triphenylphosphine) palladium (0) (11 mg, 9.94 μmol) was injected rapidly into the reaction system with a syringe. Finally, the temperature was elevated to 75 ℃ and refluxed overnight. The reduced pressure was used to remove the solvent, and the residue product was separated by silica gel column. The eluents were petroleum ether and ethyl acetate, and the volume ratio of eluent is 5:1. ^{1}H NMR (400 MHz, $CDCl_3$), δ(TMS, ppm): 4.14 (d, 2H), 7.02 (d, J = 9.28 Hz, 4H), 7.09 (s, 4H), 7.22 (t, 4H), 7.33–7.42 (m, 4H), 7.9 (m, 4H), 8.16 (s, 2H), 10.01 (s, 1H), 10.04 (s, 1H). ^{13}C NMR (100 MHz, $CDCl_3$ d6, TMS), δ(ppm): δ 163.6, 143.07, 142.57, 140.66, 140.38, 140.28, 139.83, 135.14, 135.02, 132.91, 132.02, 131.22, 130.96, 130.82, 130.2, 127.9, 127.74, 126.75, 126.13, 126.47, 119.28, 119.1, 109.99, 42.81.

2.2.4. Synthesis of FDPA

This is a substitution reaction. With addition of sodium iodide, the reactivity of CFDPA is increased, it makes CFDPA react with 2-(Aminomethyl) pyridine for producing the desired final product. The detailed procedure was listed as follows. Under nitrogen atmosphere, acetonitrile was added to a three-necked flask equipped with CFDPA (528 mg, 1 mmol), DIPEA (645 mg, 5.00 mmol) and potassium iodide (199 mg, 1.20 mmol), then the temperature condition of the reaction was kept at 40 °C for 0.5 h. After first step, 2-(Aminomethyl) pyridine was dissolved in acetonitrile, and the solution of 2-(Aminomethyl) pyridine was added to reaction solution at a slow speed and reflux for 10 h. Ten hours later, the solvent of reaction solution was removed. The residue products were removed by a small amount of the CH_2Cl_2 solution. Then, the reaction mixture was washed by saturated aqueous solution of Na_2CO_3 (90 mL) three times. The organic phase of reaction solution was dried with anhydrous sodium sulphate, and removes solvent of reaction solution. The silica column chromatography was used to remove impurities, and petroleum ether and ethyl acetate were the eluent of silica-gel chromatography, and the volume ratio of eluent is 4:1. Finally, a yellow solid was obtained. The yield of reaction product is about 75%. ^{1}H NMR (400 MHz, $CDCl_3$), δ (TMS, ppm): 3.40 (s, 1H), 3.61 (s, 1H), 3.92 (s, 1H), 4.05 (s, 1H), 7.10 (m, 4H), 7.19 (s, 1H), 7.21 (s, 1H), 7.37 (m, 8H), 7.6 (m, 8H), 7.89 (m, 4H), 8.56 (s, 1H), 9.47 (d, J = 12.72 Hz 1H), 10.02 (s, 1H). ^{13}C NMR (100 MHz, $CDCl_3$ d6, TMS), δ(ppm): δ 207.89, 169.37, 155.36, 149.55, 143.67, 141.07, 140.53, 140.21, 139.49, 136.72, 132.03, 131.39, 130.20, 128.56, 127.72, 126.47, 125.5, 122.45, 118.6, 54.63, 52.55, 34.21, 30.29, 29.67. ESI-MS (ESI, m/z): [M^+] calcd of $C_{41}H_{33}N_3O_2$, 599.26; found, 598.2502 [M - H^+]$^-$. [M^+] calcd of $C_{41}H_{33}N_3O_2$, 599.26; found, 600.2612 [M + H^+]$^+$.

2.3. Fluorescence titration studies

The metal salt solutions (10 mM) were prepared from nitrate salts (Cr^{3+}, Ca^{2+}, Mg^{2+}, Pb^{2+}, Ba^{2+}, Co^{2+}, Ni^{2+}, Cd^{2+}, Ag^+ and Cu^{2+}) and chloride salt (Zn^{2+}, Fe^{3+}, Al^{3+}, Na^+ and K^+). A probe aqueous solution (0.1 mM) of probe in THF was prepared. Fluorescence measurement was carried out with the excitation wavelength was set at 380 nm and the slit widths for excitation and emission were 5 nm/5 nm. In selective spectroscopic titration experiment, 2.4 mL of probe solution (0.1 mM) was added to a 3 cm quartz cuvette, and a 100 μL Cu^{2+} aqueous solution and 500 μL of another metal ion aqueous solution were gradually added using a micropipette and stirred to make the reaction sufficiently. In the other titration experiments, 2.9 mL of probe solution (0.1 mM) was placed in a 3 cm quartz cuvette and 100 μL different metal ions aqueous solution was added gradually by micro-pipette. Fluorescent detection conditions were the same as above.

2.4. Cytotoxicity of FDPA

For studying the biocompatibility of the FDPA in MCF-7 cell, influence of FDPA on MCF-7 cell proliferation was evaluated by MTT assay (Zhang et al., 2012; Zhang et al., 2015; Zhang et al., 2012). Briefly, MCF-7 cells were seeded in 96-well plates at a density of 5 × 10^3 cells/well, then add the Dulbecco's Modified Eagle's Medium contain 10% fetal bovine serum (FBS) into the well. The DMEM and FBS contain small amounts of calcium ions, potassium ions, magnesium ions, sodium ions and trace amounts of iron ions. The previous metal ion anti-interference experiment has proved that in the presence of a large amount of iron ions, the fluorescence intensity would be weakened, and other metal ions could not weaken the fluorescence. Therefore, the culture medium will not adversely affect the fluorescent probe.

After culturing for 24 h in cell incubator, the fusion rate of the cell was achieved 80% and the cells was fully adhered. The

96-well plates were added FDPA, and set up different FDPA concentration gradients and provided two rows of blank control group. It was used to seal the outer edge of the 96-well plate with the equal volume of PBS solution, and the same volume of pure DMEM medium was added to the two empty wells as contrast. After culturing for 24 h, 50 μL of MTT solution (5 mg/mL) was added to each well of 96-well plate. After 3 h, the liquid was removed from wells, then DMSO (200 μL/well) was added to the wells. Then it was shaken at low speed for 10 min in the shaker. After shaking, the absorbance was recorded at the 590 nm enzyme label using a microplate reader, and repeated three times. The cell viability and standard deviation were calculated by absorbance method.

2.5. Confocal microscopic imaging of cells using FDPA and copper ion

For researching the process of FDPA entering the nucleus of MCF-7 cells, it was used by confocal laser scanning microscope (CLSM Zeiss 710 3-channel, Zeiss, Germany), the excitation wavelength is 405 nm. MCF-7 cells were seeded in the laser confocal culture dish at a density of 1×10^4 cells/well, 30 μL of DMSO contains FDPA (10 μM) was added to the laser confocal culture dish. After culturing for 4 h, medium was removed by phosphate-buffered saline (PBS), then it observed and photograph probe-stained cells via CLSM. Then, cell morphology was fixed in 4% paraformaldehyde (400 μL/well), after half an hour, paraformaldehyde was removed by PBS. Subsequently, the cells were incubated with the medium contains copper salt (copper ion concentration was 20 μM) for 1 h, and then the medium was removed by PBS and paraformaldehyde. Then cell plates were observed and photographed using CLSM.

3. Results and discussion

3.1. AIE properties and size distribution

Based on the ^{1}H NMR data, we demonstrated that the fluorescent probe has been successfully synthesized. On the other hand, because the FDPA contains TPE structure, FDPA should also possess AIE feature. The self-assembly and AIE feature of FDPA was evaluated by direct dispersion of FDPA in mixture solution with 95% water. The effect on emission was investigated by changing the volume ratio of water in the probe H_2O/THF mixed solution. By increasing the volume percentage of water fractions (0–95%) to the solution of FDPA probe, a gradually increasing emission was observed at 507 nm (Fig. 1**b**). This significant enhancement of fluorescence intensity in aqueous solution is typical phenomenon for AIE compounds, absolutely fluorescence quantum yield is 65.32%, fluorescence lifetime is 1.2153 ns. On the other hand, the AIE feature of FDPA was directly observed by comparison of the photographs of FDPA suspension after UV lamp irradiation. It can be seen that almost no fluorescence was observed when the FDPA was dispersed in THF, while strong green fluorescence was emitted when the FDPA was dispersed in the mixture solution with 95% water and 5% THF.

To further verify the amphiphilicity and aggregation of the AIE probe molecules, we prepared a series of control experiments. The Br-TPE-Br is a typical molecule with AIE feature. It was precipitated, opaque and unevenly dispersed in H_2O/THF solution containing 95% water. However, the appearance of FDPA probe in the solution of 95% H_2O/THF ratio were transparent and homogeneous (Fig. 1**a**). This phenomenon can be considered as a probe molecule in the copper

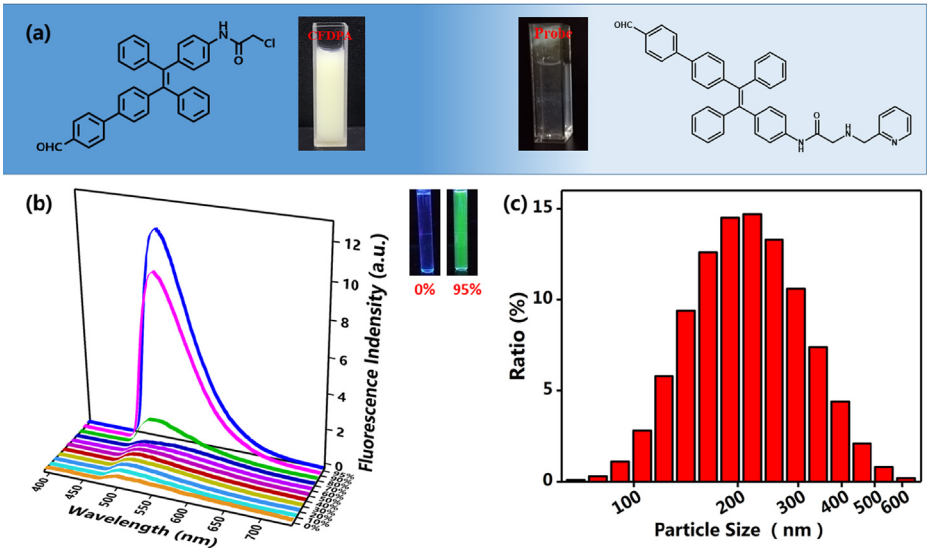

Fig 1 (a) The appearance of Br-TPE-Br and probe in the solution of 95% H_2O/THF ratio, (b) Emission fluorescence spectra of FDPA that was dispersed in the mixture of THF and water with different water fractions, the inset of figure a is the suspension of FDPA in pure organic solvent THF (left cuvette) and solution with 95% water (right cuvette) under UV lamp irradiation, (c) DLS results of FDPA in aqueous solution (100% water, removed THF before DLS test). The formation of nanoparticles would also imply the self-assembly of FDPA.

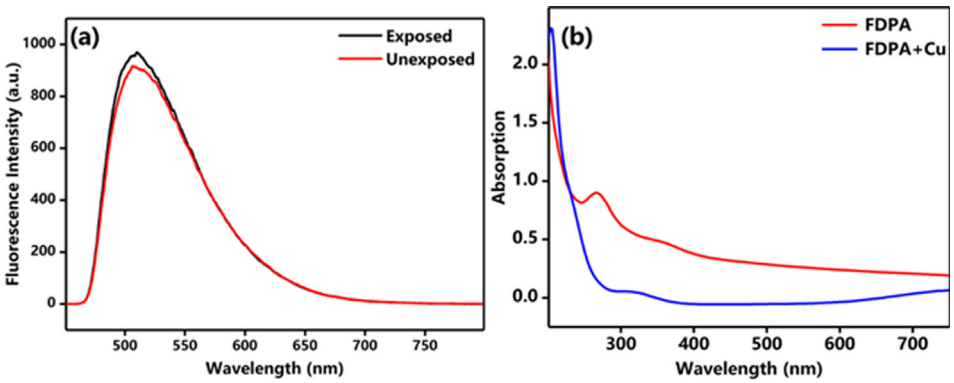

Fig 2 (a) Fluorescence stability of FDPA, (b) Ultraviolet spectrum of the probe. The solution of this test is THF/H_2O (V_{THF} : V_{water} = 5:95).

ion detection group was a hydrophilic group. It had also been reported that this phenomenon was due to the molecular aggregation suspended in the mixture was nanosize (Hong et al., 2011). This phenomenon was verified by the DLS test. We found that the formation of aggregation with sizes of probe (100 μM, 95% H_2O/THF) mainly distributing between 138 nm and 320 nm (average size 229 nm) (Fig. 1**c**), accounting for the probe molecules had assuredly aggregated into nanoparticles in mixed solution. The probe had a high fluorescence intensity due to the aggregation. In addition, it's explained that the behavior of aggregation of fluorescent probe in aqueous due to fluorescent probe consists of the fluorescence part was the hydrophobic and detection of probe group was the hydrophilic.

Fluorescence stability is a very important parameter for fluorescence sensor and biological imaging applications. In this work, the fluorescence stability of FDPA was evaluated by direct UV lamp irradiation. Herein, the FDPA was dispersed in aqueous solution, the fluorescence intensity of the suspension of FDPA before and after irradiation was measured using fluorescence spectroscopy. As shown in Fig. 2**a**, only a small decrease of fluorescence intensity was observed after the FDPA suspension was irradiated by UV lamp at 365 nm for 30 min. The fluorescence emission peak and other fluorescent properties have not obviously changed. It suggested that FDPA possesses excellent fluorescence stability and is useful for sensor and biological imaging applications. Moreover, the UV–Vis spectrum of FDPA was also determined. As shown in Fig. 2**b, a** sharp peak at 280 nm and a shoulder peak at 340 nm was found. The peak at 280 nm could be assigned to the $\pi \rightarrow \pi^*$ transition and the shoulder peak indicated the conjugation rings of FDPA. The UV spectrum also indirectly verifies the detection mechanism.

3.2. The morphology and structure of probe after self-assembly

Based on DLS results, we have known that this new compound has good dispersibility in water. In the molecular

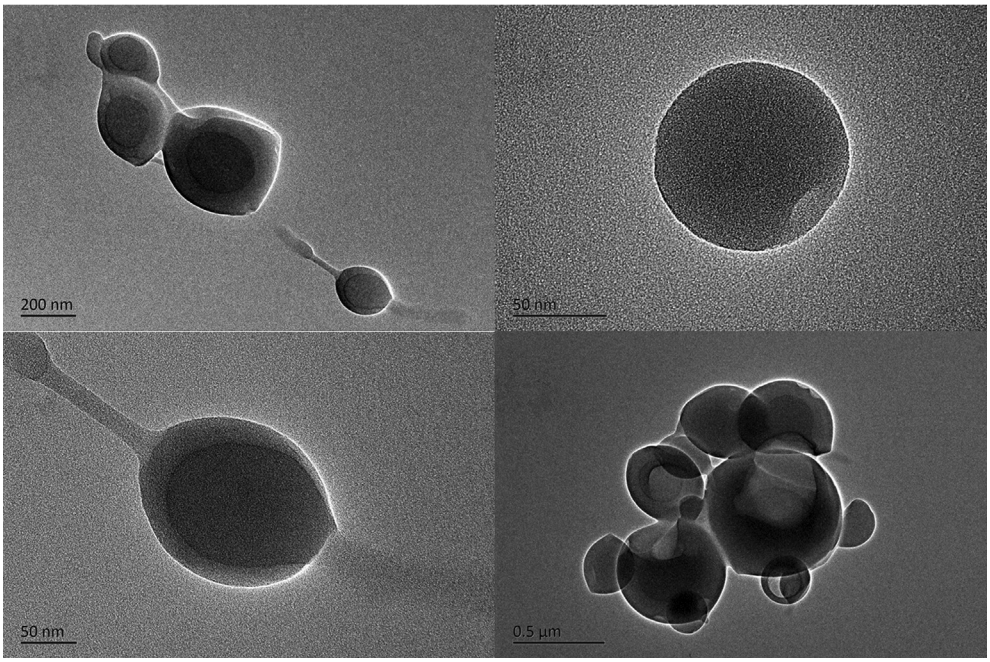

Fig 3 TEM images of FDPA with different magnifications. The TEM images implied that the amphiphilic FDPA could form the spherical nanoparticles with size between 150 and 300 nm.

structure of the compound, tetraphenylethylene of the compound is a hydrophobic unit. The probe part is the 2-picolylamine group and it is a hydrophilic unit. Take advantage of the structure of the compound, it could self-assemble in water and formation of nanoparticles with good water solubility. Therefore, the size and morphology of the aggregate of FDPA were further characterized by TEM. As shown in Fig. 3, the spherical particles were clearly observed from TEM images. The size of these particles is between 150 and 300 nm. Based on the TEM images, they clearly indicate the particles were formed via self-assembly. In these aggregates, the hydrophobic tetraphenylethylene will distributed in the core of particles, and hydrophilic group was formed the shell. We have determined the composition of FDPA by SEM-EDX. FDPA has three elements: C, N and O. The more TEM photos are provided in the supporting information (as **Fig. S16 and Table S2**). After formation of aggregates, FDPA will emit efficient in aqueous solution and exhibit high water dispersibility. The AIE and amphiphilic properties FDPA will thus endow high fluorescence intensity and good water dispersibility of the probe. This could be useful for fluorescent sensing and imaging in aqueous solution and in biological systems. Although many fluorescent sensing probes have been developed previously, the probes based on conventional organic molecules are normally show weak emission in aggregate state and thus decrease the fluorescent sensing sensitivity. In this work, the AIE-active FDPA will not only overcome the fluorescence quenching effect of probes based on conventional organic molecules, but also provide an elegant way for sensing in aqueous solution and living organisms.

3.3. The selectivity of probe towards Cu^{2+}

In order to explore the selectivity of the probe to Cu^{2+}, we investigated the effect of various metal ions (including K^+, Na^+, Zn^{2+}, Ag^+, Fe^{3+}, Al^{3+}, Cu^{2+}, Co^{2+}, Ni^{2+}, Ba^{2+}, Cr^{3+}, Cd^{2+}, Ca^{2+}, Pd^{2+}, Mg^{2+}) on fluorescence intensity of probe. Only in the presence of Cu^{2+}, the fluorescence intensity of the probe at 507 nm will be significantly weakened (Fig. 4**a**). In contrast, other metal ions have no significant quenched effect on the fluorescence intensity of the probe. This result indicated that the nitroxide ligand and the copper ion were stably bound and exhibited excellent selectivity. In order to further investigate the selectivity of the probe for copper ions in the presence of other competing metal ions. We performed a sample experiment with 1 equiv. of Cu^{2+} and 5 equiv. of other metal ions (K^+, Na^+, Zn^{2+}, Ag^+, Fe^{3+}, Al^{3+}, Co^{2+}, Ni^{2+}, Ba^{2+}, Cr^{3+}, Cd^{2+}, Ca^{2+}, Pd^{2+}, Mg^{2+}) in a solution of probe in H_2O/THF. The bar chart was obtained by integrating the fluorescence spectra of different ions (Fig. 4**b**). The results showed that the fluorescence intensity of the mixture didn't change significantly without Cu^{2+}. However, the fluorescence intensity quenched strongly when Cu^{2+} was added to the probe solution containing the competing ions. This phenomenon showed that copper ions were easier to bond with the probe, which has highly competitive. Fig. 4**c** shows the water suspensions of FDPA and after adding different metal ions. The results are well consistent with Fig. 4**a** and **b**. It can be clearly observed that the fluorescence is completely quenched after the Cu^{2+} was added in the suspension. Although the fluorescence decrease was also observed after Fe^{3+} and Co^{2+} was added into the suspension based on the image, the fluorescence could also be observed from the top of suspension. The reason is possibly ascribed to the magnetism effect of Fe^{3+} and Co^{2+}, but the impact of these ions on fluorescence intensity is little.

3.4. The LOD and the binding constant of probe

To determine the sensitivity of probe for Cu^{2+}, we designed an experiment that continuously changed the concentrations of Cu^{2+} in the fluorescence probe solution, and the fluorescence intensity at each concentration was measured by fluorescence spectroscopy. We found that the fluorescence intensities at 507 nm were rapidly decreased as the concentration of Cu^{2+}

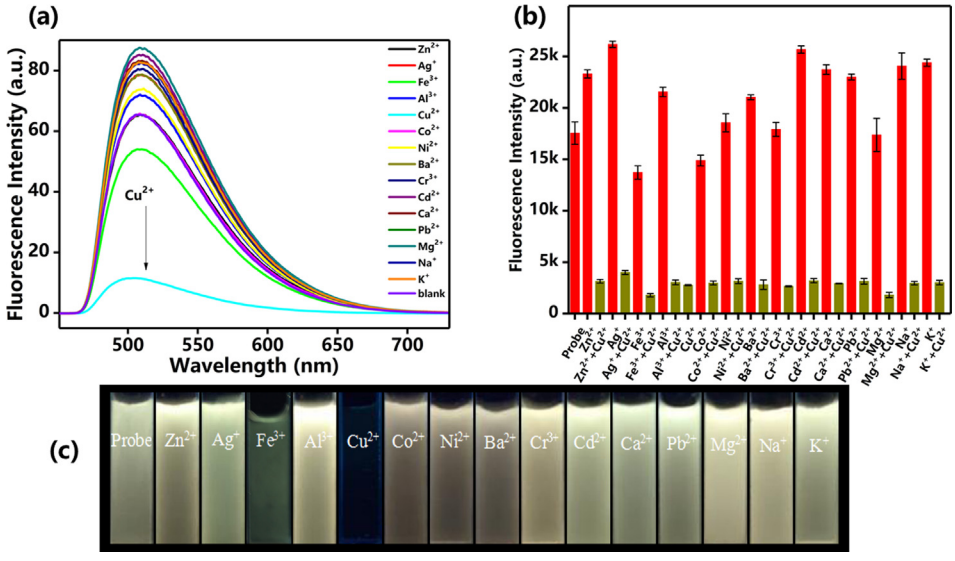

Fig 4 (a) Fluorescence spectra of FDPA upon addition of different metal ions. (b) Fluorescence intensity of probe FDPA at 532 nm with different metal ions (dark yellow lines) and after adding Cu^{2+} to the mixture of probe FDPA and different metal ions (red lines). (c) Optical images of probe in the presence of different metal ions under the UV lamp irradiation at 365 nm.

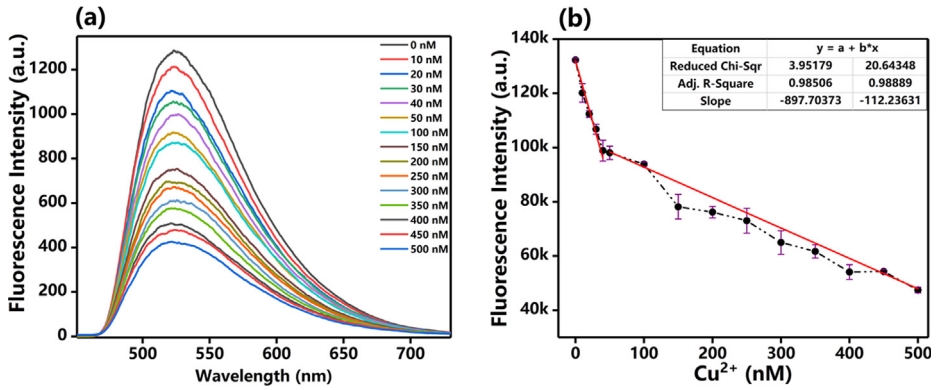

Fig 5 (a) Fl spectra of probe before and after adding different concentrations of Cu^{2+}. (b) detection concentrations of Cu^{2+} based on the changes of fluorescence intensity. The slope of first line (concentrations of Cu^{2+} ranging from 0 to 40 nM) is 897.70 (R^2 = 0.985), the slope of second line (concentrations of Cu^{2+} ranging from 50 to 500 nM) is 112.23 (R^2 = 0.989).

changed from 0 to 500 nM (Fig. 5**a**). Fluorescence intensity was almost stopped diminishing when the Cu^{2+} concentration was reached 20 μM (Fig. 5**b**). The response to Cu^{2+} is extremely sensitive. In order to calculate the limit of detection (LOD) of probe, we have adjusted the voltage of fluorescence spectrometer from 400 V to 950 V. The result of LOD was shown in **Fig. S1**. Based on the method of previous report (Wang et al., 2015), the standard curve was obtained. The LOD of probe was calculated to be 6.11×10^{-9} M. The above results demonstrated that the probe is sufficient to detect Cu^{2+} in dietary and environmental resources, and was lower than the maximum allowed levels of Cu^{2+} in drinking water (Sun and Fox, 1993).

Compared with other AIE probe, we found that LOD of this probe is significantly improved from μM to pM (Table 1). For example, in contrast to the triphenylamine type probe (Shang et al., 2021), the probe in this work has a great advantage in the LOD. This is likely due to the strong electron donate ability of TPE. The benzene ring of 4-formylphenyl has enhanced the π-conjugated system in TPE, which makes the fluorescence excitation and the emission wavelength was caused to red-shifted. It is worth noting that the MOF structure of fluorescent probe with AIE properties has excellent LOD (5.5×10^{-10}) (Xie et al., 2020). The obvious improvement LOD was possibly contributed to self-assembly of MOF. In Wang research work (Wang et al., 2020), Fe^{3+} and Fe^{2+} will interfere with the detection performance of TPE probe. However, detection speed of the probe in this work is very fast, and the interference of iron ions would almost be ignored. Moreover, we have developed another probe (Wang et al., 2021), which would detect Fe^{3+} without the interference of Fe^{2+}. Moreover, the response time is very short. When Cu^{2+} was added into the detection system, the brightness of probe would be quenched immediately. Therefore, this probe might be promising for detection of trace Cu^{2+}. The binding constant Ka was calculated based on the the stern–volmer plots (equation (1)):

$$\frac{F_0}{F} = 1 + K_a[c] \quad (1)$$

Among them, F_0 and F are the fluorescence intensities of FDPA–Cu^{2+} and the probe FDPA without Cu^{2+} in the aqueous solution. C is the concentration of Cu^{2+}. F_0 is 17551.07, F is 2803.27, C is 10^{-5} mol. The results show the K_a is 5.26×10^5 L mol^{-1}.

3.5. Sensor mechanism

In order to explore the sensing mechanism of probe to Cu^{2+}, we designed a ^1H NMR titration technique to test the ^1H NMR spectra of the probe and the probe after adding Cu^{2+} in DMSO d_6. In the ^1H NMR spectra of FDPA, the peak of the secondary amine group attached to TPE (H_a) is 10.47 ppm, the proton peak of the methine connected with nitrogen atom in the pyridine ring (H_f) was 8.5 ppm. The proton peak of the methylene connected with —NH—C═O— and imino (H_e) were located in 3.46 ppm. The peaks of the pyridine ring (H_c) were in 6.7–8.0 ppm and partially overlapped with the peaks of TPE. The peak of the hydrogen atom in the formyl group (H_b) was 10.00 ppm (Fig. 6). Interestingly, we found that the peaks in above interval were reduced or disappeared when the Cu^{2+} was added. As shown in Fig. 6 it was easy to find out that the peaks of detection group (H_a, H_d, H_f) disappeared completely. The peaks of H_f were weakened signifi-

Table 1 The comparison of LOD with other AIE probes.

Reference	LOD (mol/L)	Detection status	Molecular structure
Cai et al. (2020)	2×10^{-7}	Fluorescence turn-on	TPE—AIE
Yu et al. (2008)	2×10^{-7}	Fluorescence turn-off	Anthracene—AIE
Wang et al. (2020)	3.6×10^{-7}	Fluorescence turn-off	TPE—AIE
Xie et al. (2020)	5.5×10^{-10}	Fluorescence turn-off	MOF—AIE
Shang et al. (2021)	5.7×10^{-8}	Fluorescence turn-on	Triphenylamine—AIE
This work	6.11×10^{-9}	Fluorescence turn-off	TPE—AIE

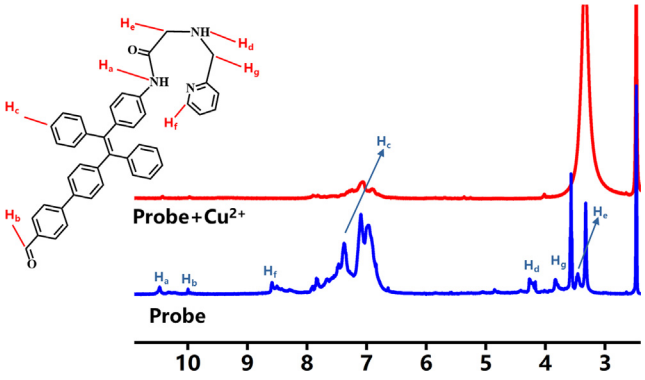

Fig 6 ^{1}H NMR spectra of FDPA and probe after adding Cu^{2+} in DMSO d_6.

cantly. It indicates that the nitrogen atom of the detection group may participate in coordination to Cu^{2+}. This situation was consistent with previous speculations. The hydrogen peak intensities were reduced at H_a, H_b, H_c, H_d and H_f. The hydrogen peaks at H_a, H_d and H_f were represented the three nitrogen atoms of the detection group. The peak intensity was weakened indicates the lone paired electron of the nitrogen atom was coordinated with the copper ion. Then the hydrogen peak was declined at H_a, H_d, and H_f, probably because of the copper ion was coordinated with the nitrogen atom, the electron mobility was suppressed in the probe group, and the original electron transfer balance was destroyed. It might be indicating that due to the complexation of copper ions with the probe, the lone paired electron forms a coordination bond with Cu^{2+}, the ICT mechanism was triggered, was leading to the energy transferred, and made the fluorescence quenched.

Previous report has demonstrated that PMQA could detect Zn^{2+} and have well water solubility, biocompatibility and responsive in a wide pH range (Zhang et al., 2013). The detection characteristic of this probe was emitted green fluorescence when it was encountered with Zn^{2+}. Normally, Cu^{2+} was the common and potent competitor of Zn^{2+} for diverse Zn^{2+} probe, but the probe was capable of detecting Zn^{2+} without being affected by Cu^{2+}. The mechanism is ascribed to the coordination of the nitrogen atom in the detection group and the oxygen atom in the carbonyl group with Cu^{2+} to form complex. We exploited this principle to redesign the fluorescent part of the probe using TPE as fluorescence group, reserve a halogen group as a stacking interface in TPE. Via the light-emitting group of the probe was changed, the probe was turned into a probe could detect Cu^{2+} rapidly, and has no response to zinc ions. Through synthesis and correlation test, we found that the probe in this work was different from that in other previous research groups. We have made the fluorescence emission wavelength further lengthened and showed yellow fluorescence at 365 nm. Without encountering Cu^{2+}, the probe would emit fluorescence, when the probe was encountering Cu^{2+}, the fluorescence should immediately quench. The reason for this phenomenon might be the probe has the internal charge transfer mechanism (ICT), and the lone paired electron in the detection group forms a coordination bond with Cu^{2+} to generate energy transfer. Therefore, when the probe was contacted with Cu^{2+} to form a complex and the fluorescence quench.

For more intuitive research on the detection mechanism, we have conducted mass spectrometry comparison tests in different solvents (THF/H_2O and DMSO). Mass spectrometry can intuitively indicate the mass before and after molecular complexation. The MS result was carried out in the THF/H_2O system solvent, and the molecular weight of the target molecule was found at 600.26. Due to the solvent has a small amount of tetrahydrofuran, LCMS could use to detect FDPA molecules dissolved in THF. Then copper ions were added into

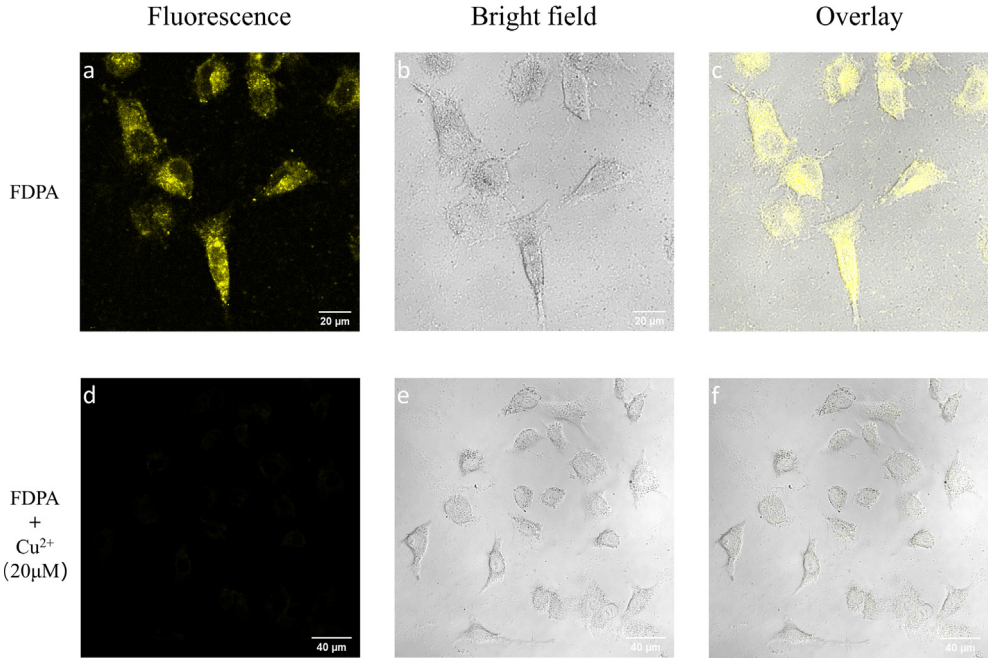

Fig 8 CLSM images of MCF-7 cells after incubation with 10 μM of FDPA for 4 h. (a) excited with 405 nm laser, (b) bright field and (c) merge image of a and b. CLSM images of MCF-7 cells after further incubation with 20 μM of Cu^{2+} for 0.5 h. (d) excited with 405 nm laser, (e) bright field and (f) merge image of d and e.

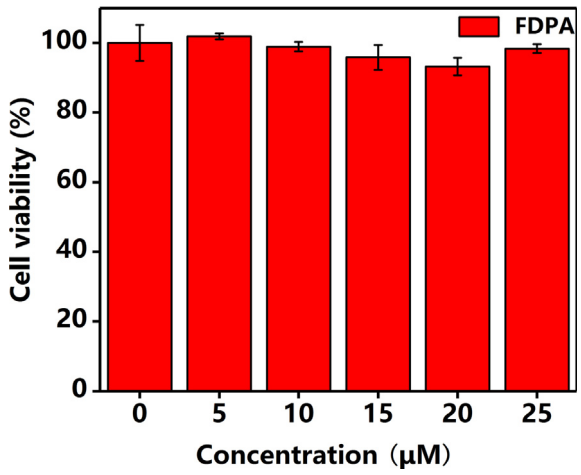

Fig 7 The viability of MCF-7 Cell after incubation for 24 h with different concentrations of FDPA. The concentrations of the FDPA are 0 μM, 5 μM, 10 μM, 15 μM, 20 μM, 25 μM, the viability values of MCF-7 Cells are 100%, 101.86%, 98.88%, 95.84%, 93.21%, 98.34%, respectively.

the solution, and the peak at 600.26 was disappeared. This phenomenon shows that when the FDPA was complexed with copper ions, the complex formed could not be dissolved in tetrahydrofuran. The FDPA has good dispersibility in aqueous solution, but it does not mean FDPA with Cu^{2+} complex dissolved in water or tetrahydrofuran, so it cannot be detected in LCMS system. Although the corresponding molecular weight peak of the complex was not found at 663, but it could be indirectly proved by mass spectrometry that the molecule can be complexed with copper ions in water after self-assembly. In order to more intuitively reflect the complex relationship between molecules, we have taken DMSO solution for the LCMS test. By comparison, it was found that before copper ions are added, there is still a peak at 600.26, and the peak at around 663 does not exist. When copper ions are added, the peak at 600.26 is almost disappeared. However, the appearance of the peak at 663 was indicated that FDPA has complexed with copper ions, but the solubility of the complex in DMSO is small, so the intensity of the peak is not very high. Based on the results from mass spectrometry, we proved that FDPA could bind with copper ions. Through the nuclear magnetic test, the complexation point of FDPA should be determined.

3.6. Cell viability evaluation

To evaluate the potential of the probe in biological system, the biocompatibility of probe is very important. Herein, the MCF-7 cells were selected as the model cells, the toxicity of the probe was examined based on the MTT method. The concentrations of probe are set at the range of 0–25 μM. After the probe was incubated with cells for 24 h, the cell viability values were calculated as compared with the control group. As displayed in Fig. 7, when the concentrations of probe increased, the cell viability values have not decreased obviously. When the concentration of the probe is as high as 25 μM, the cell viability value still kept above 90%. The cell viability evaluation results suggested that the probe possessed considerable good biocompatibility and low toxicity, indicating its potential applications in biomedical field.

3.7. Sensing of Cu^{2+} in cells

The potential utilization of FDPA for sensing the Cu^{2+} in biological system was also determined by the CLSM. Owing to the strong fluorescence intensity, the MCF-7 cells could be stained by FDPA. As displayed in Fig. 8**a**, strong and uniform yellow fluorescence could be observed. It illustrates FDPA could be internalized by the cells after 4 h incubation. Moreover, we could also observe that the cell still kept normal morphology, further indicating the low toxicity of FDPA (Fig. 8**b**). The good biocompatibility is reasonable because the dosage of probe is only 10 μM, which is much low the highest concentration for cell viability examination. It should be noted that there are some areas are lack of fluorescence signals in the central region of cells. We speculate that these regions should be the locations of cells. The sensing capability of FDPA for Cu^{2+} was also examined by CLSM. As shown in Fig. 8**d**, we can find that almost no fluorescence signals were observed form the CLSM image after the cells were incubated with FDPA and further incubated with 20 μM of Cu^{2+} for 0.5 h. The concentration of Cu^{2+} used in this work is comparable with or even lower than that used in previous reports (Wang and Wu, 2013). Therefore, the above comparison clearly indicated that the probe could be used for detection of Cu^{2+} in biological system.

4. Conclusions

In summary, we designed a TPE dye based fluorescent probe FDPA for rapid detection Cu^{2+}. The probe possesses amphiphilic properties and can be dispersed in aqueous solution and formation of nanoscale particles. We demonstrated that these self-assemblies could emit enhanced fluorescence owing to its AIE feature and good photostability, which makes them promising for sensor and biological imaging applications. Moreover, the probe would be utilized for Cu^{2+} detection with high selectivity and sensitivity. The detection limit of the probe for Cu^{2+} could reach 10^{-5} M and other heavy metal ions will not affect the detection of Cu^{2+}. This work provides a novel route for the sensor of heavy metal ions in aqueous solution through the synthesis of amphiphilic AIE-active molecules, which could be self-assembled into nanoparticles with enhanced fluorescence intensity.

CRediT authorship contribution statement

Deqiang Wang: Investigation, Methodology, Writing – original draft. **Xin Zhou:** Investigation, Methodology. **Chong Ma:** Investigation, Methodology. **Meiying Liu:** Project administration, Funding acquisition, Resources, Data curation. **Hongye Huang:** Investigation, Methodology. **Xiaoyong Zhang:** Conceptualization, Funding acquisition, Supervision, Writing – review & editing. **Yen Wei:** Conceptualization, Funding acquisition, Supervision.

Declaration of Competing Interest

The authors declare that they have no known competing financial interests or personal relationships that could have appeared to influence the work reported in this paper.

Acknowledgments

This research was supported by the National Natural Science Foundation of China (Nos. 21788102, 21865016).

Appendix A. Supplementary material

Supplementary data to this article can be found online at https://doi.org/10.1016/j.arabjc.2021.103351.

References

Aksuner, N., Henden, E., Yilmaz, I., Cukurovali, A., 2009. Dyes Pigm. 83, 211–217.
Barnham, K.J., Masters, C.L., Bush, A.I., 2004. Nat. Rev. Drug. Discov. 3, 205–214.
Becker, J.S., Matusch, A., Depboylu, C., Dobrowolska, J., Zoriy, M. V., 2007. Anal. Chem. 79, 6074–6080.
Cai, Y., Fang, J., Zhu, H., Qin, W., Cao, Y., Yu, H., Shao, G., Liu, Y., Liu, W., 2020. Sens. Actuators, B 303, 127214.
Cao, Q.-Y., Jiang, R., Liu, M., Wan, Q., Xu, D., Tian, J., Huang, H., Wen, Y., Zhang, X., Wei, Y., 2017. Mater. Sci. Eng. C-Mater. 80, 578–583.
Cao, Q.-Y., Jiang, R., Liu, M., Wan, Q., Xu, D., Tian, J., Huang, H., Wen, Y., Zhang, X., Wei, Y., 2017. Mater. Sci. Eng. C-Mater. 80, 411–416.
Dou, J., Gan, D., Huang, Q., Liu, M., Chen, J., Deng, F., Zhu, X., Wen, Y., Zhang, X., Wei, Y., 2019. Inter. J. Biolog. Macromol. 136, 476–485.
Hong, Y., Chen, S., Leung, C.W., Lam, J.W., Liu, J., Tseng, N.W., Kwok, R.T., Yu, Y., Wang, Z., Tang, B.Z., 2011. ACS Appl. Mater. Interfaces 3, 3411–3418.
Huang, Q., Zhao, J., Liu, M., Chen, J., Zhu, X., Wu, T., Tian, J., Wen, Y., Zhang, X., Wei, Y., 2018. J. Taiwan Inst. Chem. E. 82, 92–101.
Huang, Q., Zhao, J., Liu, M., Li, Y., Ruan, J., Li, Q., Tian, J., Zhu, X., Zhang, X., Wei, Y., 2018. J. Taiwan Inst. Chem. E. 86, 174–184.
Jiang, Y., Chen, Y., Alrashdi, M., Luo, W., Tang, B.Z., Zhang, J., Qin, J., Tang, Y., 2016. RSC Adv. 6, 100318–100325.
Jiang, R., Liu, M., Li, C., Huang, Q., Huang, H., Wan, Q., Wen, Y., Cao, Q.-Y., Zhang, X., Wei, Y., 2017. Mater. Sci. Eng. C-Mater. 80, 708–714.
Jiang, R., Liu, H., Liu, M., Tian, J., Huang, Q., Huang, H., Wen, Y., Cao, Q.-Y., Zhang, X., Wei, Y., 2017. Mater. Sci. Eng. C-Mater. 81, 416–421.
Kaur, M., Min, J.C., Dong, H.C., 2016. Dyes Pigm. 125, 1–7.
Khandare, D.G., Joshi, H., Banerjee, M., Majik, M.S., Chatterjee, A., 2014. RSC Adv. 4, 47076–47080.
Kong, R.-M., Zhang, X., Ding, L., Yang, D., Qu, F., 2017. Anal. Bioanal. Chem. 409, 5757–5765.
Li, H., Zhang, X., Zhang, X., Yang, B., Yang, Y., Wei, Y., 2014. Polym. Chem. 5, 3758.
Li, J.-J., Zhu, L.-T., Luo, Z.-H., 2016. Chem. Eng. J. 287, 474–481.
Liu, Y.L., Lv, X., Zhao, Y., Chen, M.L., Liu, J., Wang, P., Guo, W., 2012. Dyes Pigm. 92, 909–915.
Liu, J., Qian, Y., 2017. Dyes Pigm. 136, 782–790.
Liu, Y.-L., Wang, Z.-K., Qin, W., Hu, Q.-L., Tang, B.Z., 2017. Chin. J. Polym. Sci. 35, 365–371.
Lutsenko, S., Gupta, A., Burkhead, J.L., Zuzel, V., 2008. Arch. Biochem. Biophys. 476, 22–32.
Mahato, P., Saha, S., Suresh, E., Di Liddo, R., Parnigotto, P.P., Conconi, M.T., Kesharwani, M.K., Ganguly, B., Das, A., 2012. Inorg. Chem. 51, 1769–1777.
Maurya, N., Singh, A.K., 2017. Dyes Pigm. 147, 484–490.
Moreda, A., 2005. Anal. Chim. Acta 536, 213–218.
O'Halloran, A.V.D., Thomas, V., 2008. Nat. Chem. Biol. 4, 148–151.
Padhan, S.K., Murmu, N., Mahapatra, S., Dalai, M.K., Sahu, S.N., 2019. Mater. Chem. Front. 3, 2437–2447.
Park, G.J., Hwang, I.H., Song, E.J., Kim, H., Kim, C., 2014. Tetrahedron 70, 2822–2828.
Pourreza, N., Hoveizavi, R., 2005. Anal. Chim. Acta 549, 124–128.
Prohaska, J.R., Gybina, A.A., 2004. J. Nutr. 134, 1003–1006.
Qin, X., Wang, S., Luo, L., He, G., Sun, H., Gong, Y., Jiang, B., Wei, C., 2018. RSC Adv. 8, 31231–31236.
Que, E.L., Domaille, D.W., Chang, C.J., 2008. Chem. Rev. 108, 1517–1549.
Sen Gupta, A., Paul, K., Luxami, V., 2017. Sensor Actuat. B-Chem. 246, 653–661.
Sen Gupta, A., Paul, K., Luxami, V., 2017. Sens. Actuators, B 246, 653–661.
Shan, Y.R., Yao, W.J., Liang, Z.Q., Zhu, L.H., Yang, S.B., Ruan, Z. J., 2018. Dyes Pigm. 156, 1–7.
Shang, J.Y., Li, Y., Chen, K., Li, H., 2021. Chem. Pap. https://doi.org/10.1007/s11696-020-01447-0.
Shultz, D.A., Fox, M.A., 1989. ChemInform, 20.
Shyamal, M., Mazumdar, P., Maity, S., Samanta, S., Sahoo, G.P., Misra, A., 2016. ACS Sensors 1, 739–747.
Situ, B., Zhao, J.M., Lv, W.F., Liu, J.M., Li, H.K., Li, B., Chai, Z.X., Cao, N.N., Zheng, L., 2017. Sensor Actuat. B-Chem. 240, 560–565.
Sun, Y.P., Fox, M.A., 1993. J. Am. Chem. Soc. 115, 747–750.
Thavornpradit, S., Sirirak, J., Wanichacheva, N., 2016. J Photoch. Photobio. A 330, 55–63.
Tong, H., Hong, Y., Dong, Y., Haussler, M., Lam, J.W., Li, Z., Guo, Z., Guo, Z., Tang, B.Z., 2006. Chem. Commun. (Camb.). https://doi.org/10.1039/b608425g, 3705-3707.
Wang, Y., Liu, S., Chen, H., Liu, Y., Li, H., 2017. Dyes Pigm. 142, 293–299.
Wang, Y., Hao, X., Liang, L., Gao, L., Ren, X., Wu, Y., Zhao, H., 2020. RSC Adv. 10, 6109–6113.
Wang, H., He, Y., Li, Y., Zhang, C., Zhang, P., Cui, J., Long, Y., Chen, S., Zeng, R., Chen, J., 2019. Anal. Bioanal. Chem. 411, 1979–1988.
Wang, D., Ma, C., Zhou, X., Long, W., Liu, M., Zhang, X., Wei, Y., 2021. Colloid Interface Sci. Commun. 40, 100358.
Wang, H., Wang, B., Shi, Z., Tang, X., Dou, W., Han, Q., Zhang, Y., Liu, W., 2015. Biosens. Bioelectron. 65, 91–96.
Wang, Z., Wang, Y., Liu, G., 2016. Angew. Chem. Int. Ed. 55, 1291–1294.
Wang, H.-F., Wu, S.-P., 2013. Sensor. Actuat. B-Chem. 181, 743–748.
Xie, S., Liu, Q., Zhu, F., Chen, M., Wang, L., Xiong, Y., Zhu, Y., Zheng, Y., Chen, X., 2020. J. Mater. Chem. C 8, 10408–10415.
Xu, J.P., Song, Z.G., Fang, Y., Mei, J., Jia, L., Qin, A.J., Sun, J.Z., Ji, J., Tang, B.Z., 2010. Analyst 135, 3002–3007.
Xue, X.L., Fang, H.B., Chen, H.C., Zhang, C.L., Zhu, C.C., Bai, Y., He, W.J., Guo, Z.J., 2016. Dyes Pigm. 130, 116–121.
Yan, L., Wen, X., Fan, Z., 2020. Anal. Bioanal. Chem. https://doi.org/10.1007/s00216-019-02378-w, 1-11.
Yu, M., Shi, M., Chen, Z., Li, F., Li, X., Gao, Y., Xu, J., Yang, H., Zhou, Z., Yi, T., Huang, C., 2008. Chem. Eur. J. 14, 6892–6900.
Yu, Z., Yun, F.F., Gong, Z., Yao, Q., Dou, S., Liu, K., Jiang, L., Wang, X., 2017. J. Mater. Chem. A 5, 10821–10826.
Yuan, B., Wang, D.X., Zhu, L.N., Lan, Y.L., Cheng, M., Zhang, L. M., Chu, J.Q., Li, X.Z., Kong, D.M., 2019. Chem. Sci. 10, 4220–4226.
Zhang, L., Cui, X., Sun, J., Wang, Y., Li, W., Fang, J., 2013. Bioorg. Med. Chem. Lett. 23, 3511–3514.
Zhang, X., Qi, H., Wang, S., Feng, L., Ji, Y., Tao, L., Li, S., Wei, Y., 2012. Toxicol. Res. 1, 201–205.
Zhang, X., Hu, W., Li, J., Tao, L., Wei, Y., 2012. Toxicol. Res. 1, 62–68.
Zhang, X., Liu, M., Zhang, X., Deng, F., Zhou, C., Hui, J., Liu, W., Wei, Y., 2015. Toxicol. Res. 4, 160–168.
Zhang, X., Huang, Q., Liu, M., Tian, J., Zeng, G., Li, Z., Wang, K., Zhang, Q., Wan, Q., Deng, F., 2015. Appl. Surf. Sci. 343, 19–27.